



brain cells, as well as with neuroprotective effects against neurological damage [7]. Albeit *in silico* observations have shown the potential of different STLs from root chicory to permeate the blood-brain barrier (BBB) [8], the brain uptake of these STLs and their effect on BBB permeability has not been directly examined, so far.

The BBB is the physiological barrier located between the blood and the brain parenchyma. The BBB is formed by brain microvascular endothelial cells (BMECs) that are surrounded by astrocyte foot processes and pericytes. This unique structure accounts for the restricted permeability of the brain microvasculature, which has the key function of protecting the brain, namely by preventing the crossing of several molecules (e.g., toxins) [9]. In turn, the BBB constitutes the major obstacle for any molecule to reach the brain, a massive hurdle for developing brain-targeted therapies. There are several proposed mechanisms by which a small molecule can cross the BBB [10]. Thus, the exchange of molecules between the bloodstream and the brain requires an efficient transport across the BBB that is mediated by many different mechanisms which may occur by paracellular or transcellular routes [10].

Small, lipophilic molecules could cross the endothelium by diffusion, whereas other molecules enter the brain by transporter-mediated processes, which can be categorized as carrier-mediated, adsorptive transcytosis, or receptor-mediated transcytosis. On the other hand, the ATP-binding cassette (ABC) proteins are the major efflux transporters at the BBB level, which limit the brain entrance of multiple toxins, drugs, and endogenous metabolites toward the brain [11]. Another important transcellular route involves the adsorptive transcytosis process and receptor-mediated transcytosis. In this sense, caveolar-mediated transcytosis is the primary mechanism of traffic of substances across the BBB [12], where caveolin-1 is the major component of caveolar vesicles.

The paracellular transport is restricted by tight junctions (TJs), which tightly connect brain capillary endothelial cells to maintain the strength of the BBB, being TJs proteins like zonula occludens (ZO)-1 used as biomarkers of the BBB integrity [10]. Other important group of proteins are those forming adherens junctions (AJs), which give place to a continuous belt, between adjacent endothelial cells and contribute to the regulation of paracellular permeability [9]. For instance,  $\beta$ -catenin is a key AJs protein in the BBB, and its upregulation has been suggested for the maintenance of TJs protein assembly and barrier function. Moreover, it has been described that an increase of TJs and AJs protein expression alleviated the cerebral inflammatory response after traumatic brain injury by protecting the BBB [13].

Until today, as per the best of our knowledge, the effects of STLs at the BBB level have not been evaluated. Since novel advances in our understanding of whether these molecules cross the BBB and their function would help for developing innovative approaches by targeting the brain circuits, the major aims of this work were to evaluate: i) effects of different STLs in the tightness (i.e., integrity) of the BBB, ii) BBB permeation of STLs and the role of the caveolae-mediated transcytosis transport route in the BBB, and iii) the specific effects of those compounds in the main TJs and AJs expression in the BBB. Advances in our understanding whether these molecules cross the BBB and their function in the BBB would help for developing innovative approaches for delivering drugs to brain circuits.

## 2. Material and methods

### 2.1. Chemical and reagents

Lactucin (LC), lactucopicrin (LCP), 11 $\beta$ -13-dihydroxylactucin (DHLC) and 11 $\beta$ -13-dihydroxylactucopicrin (DHLCP) were acquired from Extrasynthese (3809, 3813, 3810, 3811) (Genay Cedex, France). Costunolide (COS), parthenolide (PAR), dimethyl sulfoxide (DMSO) ( $\geq 99.9\%$ ), Hanks' balanced salt solution (HBSS) and tween-20 were obtained from Sigma Aldrich (St. Louis, MO, USA). Tris-base and glycine were purchased from Carl Roth (Karlsruhe, Germany). HPLC grade acetonitrile

and acetic acid were obtained from Merck (Saint Louis, MO, USA). Milli-Q water purification system (Merck Millipore, Billerica, MA, USA) was used in all experiments.

### 2.2. HBMEC cell line

Confluent cultures of human BMECs (HBMECs) were used as a simplified *in vitro* model of the BBB. The cells were grown as previously [14]. Before the experiments, inserts and plates were coated with rat-tail collagen-I (BD Biosciences, Erembodegem, Belgium). All the compounds used in the experiments were solubilized in DMSO (<0.5%) and filter sterilized (0.22  $\mu$ m). All experiments were performed between cell passages 22 and 27.

#### 2.2.1. BBB transport assays

HBMECs were plated on 12 well-transwell® plates (12 mm, 0.4  $\mu$ m Pore Polyester Membrane Insert). Confluent monolayers of HBMECs were established 5 days after seeding. Transport assays were conducted in HBSS, supplemented with 0.1% fetal bovine serum (FBS). HBMECs were incubated with 5  $\mu$ M of each STL in the apical side for 2 h. Monolayer integrity was ensured in all experiments as described in the Section 2.2.2.

To evaluate the transport of the STLs, the supernatant samples from upper (apical) and lower (basolateral) sites were collected and kept at  $-80\text{ }^{\circ}\text{C}$  until the LC-Orbitrap MS analysis. Endothelial transport was calculated as a percentage determined by the ratio of lower compartment concentration and the sum of upper and lower compartments concentrations, as before [14].

#### 2.2.2. BBB integrity

Sodium-fluorescein (Na-F) paracellular permeability and trans-endothelial electrical resistance (TEER) were measured, as previously reported [14], to ensure the BBB integrity as well as that the crossing of the compounds was not due to BBB disruption. The endothelial permeability coefficient  $P_e$  was calculated as a percentage of variation from control (CT). TEER readings were performed using an EVOM3 Epithelial Volt Ohm Meter (World Precision Instruments, Inc., USA). Readings were collected before adding the compounds (0 h) and 2 and 6 h afterwards.

#### 2.2.3. LC-Orbitrap-FTMS analysis

For the detection of STLs, 600  $\mu$ L of the apical and basolateral samples were evaporated in a speedvac (Savant SC100, Thermo Fischer Scientific) and resuspended in 200  $\mu$ L 80% methanol containing 0.1% formic acid. The extracts were prepared by brief vortex and sonication for 15 min. Next, the extracts were centrifuged at 21,000  $\times$  g at room temperature and the clear supernatant was used for LC-MS analysis. LC-MS analysis was performed using a LC-PDA-LTQ-Orbitrap FTMS system (Thermo Fischer Scientific), which consists of an Acquity UPLC (H-Class) with Acquity elambda photodiode array detector (220–600 nm) connected to a LTQ/Orbitrap XL hybrid mass spectrometer equipped with an electrospray ionizer (ESI). The injection volume was 5  $\mu$ L. Chromatographic separation was on a reversed phase column (Luna C18/2,3  $\mu$ m, 2.0  $\times$  150 mm; Phenomenex, USA) at 40  $^{\circ}\text{C}$ . Degassed eluent A [ultra-pure water: formic acid (1000:1, v/v)] and eluent B [acetonitrile:formic acid (1000:1, v/v)] were used at a flow rate of 0.19 mL min $^{-1}$ . A linear gradient from 5% to 75% acetonitrile (v/v) in 45 min was applied, which was followed by 15 min of washing and equilibration. FTMS full scans ( $m/z$  90.00–1350.00) were recorded with a resolution of 60,000 FWHM. Quantification was performed by peak area quantification in using the batch Thermo Xcalibur 4.0.27.19 software (Thermo Fischer Scientific) using accurate mass of STLs with 5 ppm accuracy. The peak area was compared to a standard curve prepared as a dilution series of authentic standards.

#### 2.2.4. Fluorescence microscopy

HBMECs were seeded on 24-well plates with collagen type I-coated coverslips (25,000 cells/well) and grown for 5 days. After the STL treatments, the cells were fixed with paraformaldehyde 4 %, washed 3 times with PBS, and maintained in PBS at 4 °C until the immunostaining protocol, performed no longer than 2 weeks. For the immunostaining, the coverslips were incubated overnight at 4 °C with primary antibodies: ZO-1 polyclonal antibody (#61-7300, 1:100, Invitrogen), caveolin-1 polyclonal antibody (#3238, 1:300, Cell Signaling Technology),  $\beta$ -catenin polyclonal antibody (#PA5-16429, 1:100, Invitrogen) and P-gp monoclonal antibody (#MA1-26528, 1:50, Invitrogen). The secondary antibodies were Alexa Fluor 594 goat anti-rabbit IgG (#A-11012, 1:500, Invitrogen) or Alexa Fluor 568 goat anti-mouse IgG (#A-11031, 1:500, Invitrogen) and the incubation was performed for 1 h at room temperature, in the dark. Nuclei were counterstained using Invitrogen™ ProLong Gold Antifade Mountant with DAPI. Between incubations, cells were washed three times with PBS. Negative controls (without primary antibody incubation) were also performed (data not shown). HBMEC images were acquired using a Microscope: Zeiss Axioimager Z2 (Zeiss, Germany), using 40 X or 63 X (for P-gp expression) oil immersion objectives. Four fields per condition were acquired and evaluated for semi-quantitative analysis. Immunofluorescence images obtained by fluorescence microscopy were examined using Icy (Institute Pasteur and France BioImaging, Paris, France) and ImageJ (National Institutes of Health, Bethesda, MD, USA) softwares.

Membrane, nuclei, and total cell fluorescence intensity were quantified using 10 cells per field in which the area, ellipse, and polygon tools were used, respectively, from Icy software.

$\beta$ -catenin fluorescence values were acquired per field (10 cells/4 fields) through the total intensity of circled cell intensity. For ZO-1, both membrane and cell mean fluorescence intensity, as well as membrane gaps, were quantified in 10 cells per field, using Icy software. Caveolin-1 and P-gp were quantified using Spot Detector tool from Icy software, considering 3 pixel size parameter. The representative images for all evaluated proteins were obtained in ImageJ software.

#### 2.2.5. Western blotting

HBMECs were seeded on 12-well plates (40,000 cells/well) and grown for 4–5 days. HBMEC protein extraction was performed with lysis buffer (Cell Signaling Technology). Samples (10  $\mu$ g) and Protein Marker VI (#10-245) prestained (Panreac Applichem, Darmstadt, Germany) were separated by SDS-PAGE gels with 8 or 10 % gradient for 120 min at 90 V in running buffer (25 mM Tris, 192 mM glycine, 0.1 % SDS, pH 8.3). Proteins were transferred to Trans-Blot Turbo Mini 0.2  $\mu$ m polyvinylidene fluoride (PVDF) membranes using the Bio-Rad Trans-Blot Turbo Transfer System for 7 min. Membranes were blocked with 5 % non-fat milk (caveolin-1) or 5 % BSA in TBST (20 mM Tris, 150 mM NaCl, containing 0.05 %). Primary antibodies were incubated overnight at 4 °C, followed by secondary antibodies (horseradish peroxidase conjugated, ECL anti-rabbit IgG; Sigma-Aldrich Missouri, EUA), incubated for 1 h at room temperature. The blots were probed with GAPDH Monoclonal Antibody (#AM4300, Invitrogen, 1:5000), as a loading control. Primary antibodies used for protein detection were: caveolin-1 (#3238, Cell Signaling Technology, 1:1000), ZO-1 (#61-7300, Invitrogen, 2  $\mu$ g/mL), and  $\beta$ -catenin (#PA5-16429, Invitrogen, 1  $\mu$ g/mL). Membranes were developed using Amersham ECL Prime Western Blotting Detection Reagent (GE Healthcare) and chemiluminescence or fluorescence scanned with LI-COR Odyssey Infrared Imaging System (LI-COR, Lincoln, NE) and analysed by Image Studio Lite Version 5.2 software (LI-COR).

#### 2.3. Statistical analysis

The data were processed in Microsoft Excel (v2209) (Microsoft, Albuquerque, NM, USA). All statistical analysis was performed using GraphPad Prism 9.0 (GraphPad Software Inc., San Diego, CA, USA).

Parametrical data were submitted to one-way ANOVA followed by Tukey post-hoc test, and non-parametrical data were under Kruskal-Wallis test with post-Dunnett's multiple comparisons, with a significance level fixed at 95 % ( $p < 0.05$ ). All the results were expressed as the mean  $\pm$  standard deviation (SD). All the experiments were performed for at least three independent biological replicates, with at least two technical replicates per condition. The outliers were identified using ROUT method from GraphPad Prism 9.0.

### 3. Results

#### 3.1. Sesquiterpene lactones (STLs) are transported across the BBB

Lactucin (LC), lactucopicrin (LCP), 11 $\beta$ ,13-dihydroxylactucin (DHLC), 11 $\beta$ ,13-dihydroxylactucopicrin (DHLCP), costunolide (COS) and parthenolide (PAR) are considered STLs with well-described anti-inflammatory and neuroprotective pharmacological properties. However, whether these molecules can cross the BBB has not been evaluated so far. In order to disclose the BBB permeability of these six STLs (Fig. 1A), 5  $\mu$ M was chosen as the highest non-toxic concentration of all the compounds in HBMECs after 6 h of incubation (Supplementary Fig. 1).

A well-validated HBMEC two-chamber BBB model was used [14]. The STLs were added to the upper chamber (apical side), mimicking the blood site, where the HBMECs formed a monolayer. Their putative transport through the BBB from "blood" to the "brain" was assessed based on quantification of each compound in both compartments after 2 h of incubation (Fig. 1B) by LC-MS. Different percentages of BBB transport were observed for each one of the STLs evaluated (Fig. 1C), suggesting that these compounds transported from the blood to the brain differently. Whereas COS showed a transport efficiency of 25.8 %, being the compound most effectively transported, PAR was the second compound that showed the greatest capacity to be transported (14.5 %). Nonetheless, LC, DHLC, and DHLCP showed values of transport close to PAR. LCP displayed the lowest capacity to cross the BBB, with an almost negligible BBB transport of 0.33 %.

In order to ensure that the differences in BBB transport did not derive from alterations in the integrity of the BBB, the paracellular permeability of Na-F was assessed in all the conditions (Fig. 1D). The results showed that any of the treatments increased the Na-F permeability compared with the untreated cells (CT), reflecting that the crossing of these compounds from the "blood" to the "brain" was not a consequence of an eventual disruption of the BBB. Surprisingly, COS and PAR treatments showed a significant ( $p < 0.05$ ) decrease of the Na-F paracellular permeability, which may suggest that COS and PAR by reducing the permeability between adjacent cells, may be increasing BBB tightness.

Knowing these STLs' BBB permeability after 2 h, we decided to evaluate whether these STLs sustain the effects for a more prolonged time. We observed that, after 6 h of incubation, the paracellular permeability of Na-F in presence of these STLs remained lower than in CT cells ( $p < 0.05$  and  $p < 0.01$  for COS and PAR, respectively Fig. 1E). Accordingly, the barrier integrity was also confirmed by measurement of the transendothelial electrical resistance (TEER) values at 0, 2 and 6 h (Fig. 1F). After 2 h of incubation, COS and PAR showed higher TEER values than in the CT cells, albeit only PAR showed statistical significance ( $p < 0.05$ ) compared to CT. Nonetheless, both COS and PAR increased TEER in HBMECs at 6 h of incubation ( $p < 0.05$ ), which reinforces the enhanced barrier tightness promoted by these STLs.

Altogether, our observations support the hypothesis that some STLs present in chicory are BBB-permeant compounds, and also could be new promising compounds to boost the BBB by improving the barrier tightness.

#### 3.2. HBMECs metabolize STLs in glutathione conjugates

In order to perceive if the differences in BBB transport of STLs could derive from the appearance of new end-route metabolites at "blood" or

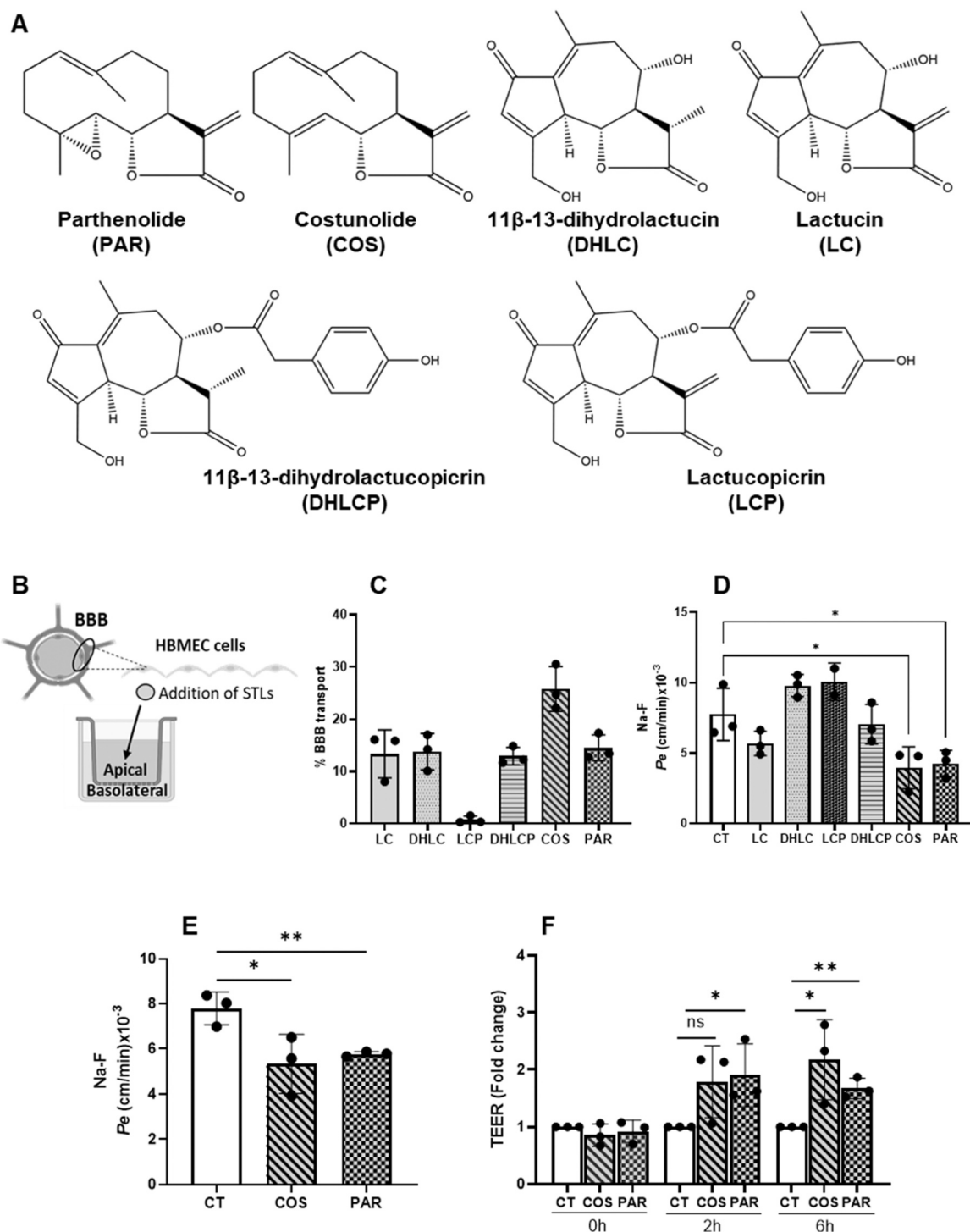


**Fig. 1.** Performance of sesquiterpene lactones (STLs) in the blood-brain barrier (BBB). (A) Chemical structures of the STLs tested in this study. (B) Experimental design used to assess the transport of STLs across HBMECs as an *in vitro* model of the BBB. (C) Endothelial transport of the STLs after 2 h of incubation. Endothelial transport is presented as percentage (%) determined by the ratio of the lower compartment concentration and the sum of the upper and lower compartments concentrations. (D) Mean of apparent permeability coefficient ( $Pe$ ) values for Na-F at 2 h for vehicle with 0.5 % DMSO (control, CT) and for all STLs. (E)  $Pe$  values for Na-F at 6 h for CT, COS and PAR. (F) Transendothelial electrical resistance (TEER) in HBMECs for CT, COS and PAR at different time-points. Statistical differences are denoted as \* $p < 0.05$  or \*\* $p < 0.01$  relatively to CT. All data are presented as means  $\pm$  SD ( $n = 3-4$ ).

“brain” sides by phase II metabolism already described for HBMECs, LC-MS analysis using Orbitrap-FTMS was performed (Fig. 2; Supplementary Fig. 2). The LC-Orbitrap-FTMS analysis revealed that, besides free STLs, also glutathione S-conjugates (GSH) of different STLs were detected after 2 h of incubation with the HBMECs. The appearance of conjugates was detected predominantly in the apical side.

Unfortunately, due to the lack of the GSH metabolites standards, the formation of these metabolites could not be quantified, which hampered the possibility to quantitatively compare the different compounds metabolism by HBMECs.

Although the formation of other potential phase-II metabolites as glucuronides, sulphates and cysteine conjugates has been previously

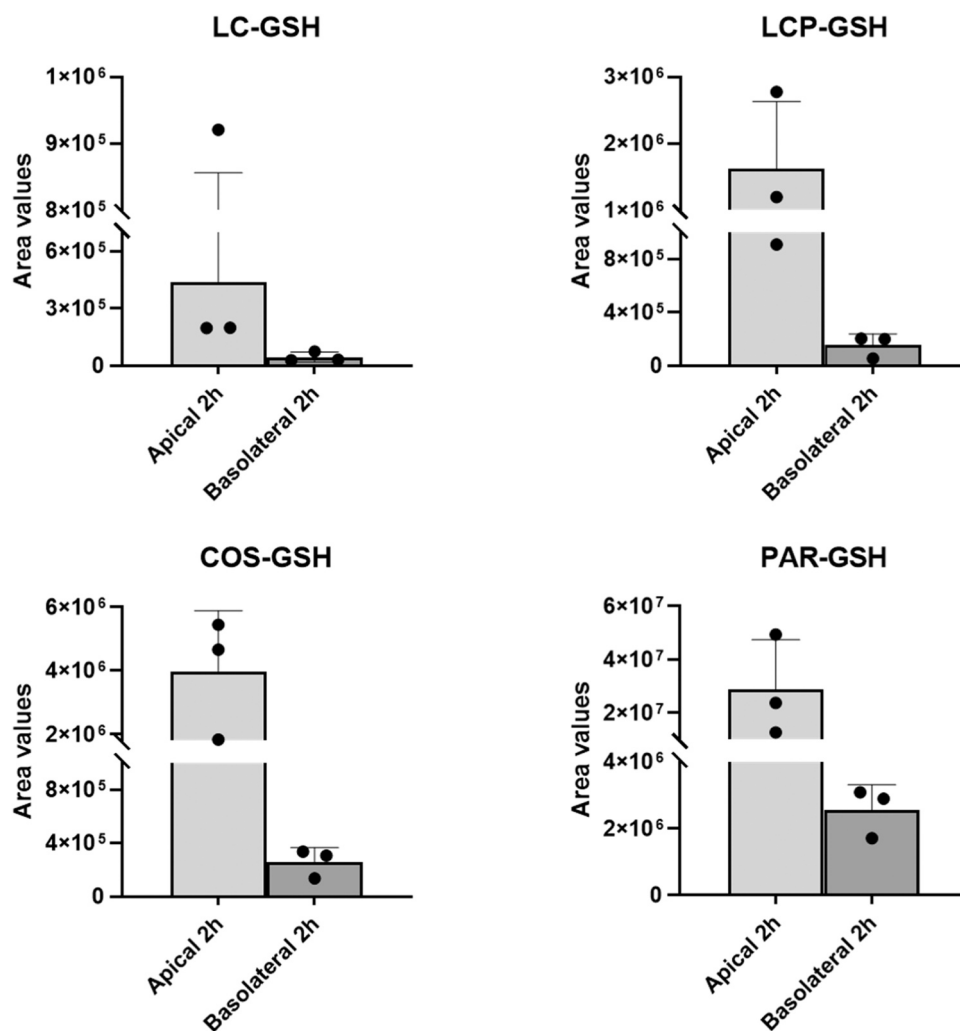


**Fig. 2.** Formation of glutathione S-conjugates (GSH) with different STLs in HBMECs. Presence of GSH-conjugates after 2 h of incubation with lactucin (LC), lactucopicrin (LCP), costunolide (COS) and parthenolide (PAR) at 5  $\mu$ M in the apical and basolateral sides of the BBB *in vitro* model.

reported in HBMECs [14], we did not detect these conjugates in our study. However, we cannot discard potential formation of other STL conjugates for longer incubation times.

It should also be pointed out the low amount of GSH conjugates in the basolateral side vs apical side after 2 h of incubation with the STLs (Fig. 2). This fact could be explained, at least in part, due to the normal GSH turnover process to maintain cell homeostasis [15] or even as an important detoxification mechanism by the cells [16].

Overall, our results show the formation of GSH conjugates from different STLs by HBMECs. These metabolites appear in the “blood” side but eventually can also be transported towards the “brain” side. Therefore, the possible bioactivities of these conjugates deserve further exploration at the BBB and brain levels.

### 3.3. Caveolae vesicles formation is promoted in the presence of COS and PAR

Transcytosis is the transcellular transport of molecules *via* vesicles, with caveolin-1 being the major structural protein of caveolae, which are critically involved in vesicular trafficking and cell signalling (*i.e.*, drug delivery through the BBB). Since COS and PAR are lipidic molecules here shown to cross the BBB, we decided to evaluate if these STLs could alter caveolin-1-positive vesicles' formation and/or expression (Fig. 3).

As shown in the immunofluorescence images, both with COS and

PAR treatments for 2 h a significant increase ( $p < 0.001$ ) in caveolin-1-positive vesicles was observed (Fig. 3A, B), albeit overall protein levels of caveolin-1 were not affected by the treatments (Fig. 3C). Moreover, the spot analysis of caveolin-1-positive vesicles demonstrated an increase in the total number of caveolae in HBMECs when exposed both COS and PAR (Fig. 3D, E), without alteration in the vesicle size (Fig. 3F).

Previous studies have described a physical interaction between P-gp and caveolin-1, and that the interaction leads to a down-regulation of P-gp function [17]. Since P-gp is primarily localized in the plasma membrane, its presence in other cellular compartments (like the Golgi and endoplasmic reticulum) have also been reported [18]. Thus, we aimed to elucidate the impact of COS and PAR on P-gp, *via* immunofluorescence analysis in HBMECs.

From our data, no major changes were observed in the P-gp localization in the cells with the different treatments (Fig. 3G). Nonetheless, from the semi-quantitative analysis, we observed a reduction in P-gp immunoreactivity following incubation with either 5  $\mu$ M of COS or PAR (Fig. 3H). These findings may point to a reduction of P-gp with both STL treatments.

Collectively, our results suggest an association between transcellular hyperpermeability (*via* an increase in caveolae vesicles formation) of these compounds across the BBB concomitant with P-gp reduced expression. These findings support the role that caveolin-1 may have in the transport towards the brain observed for COS and PAR at 2 h (Fig. 1C).

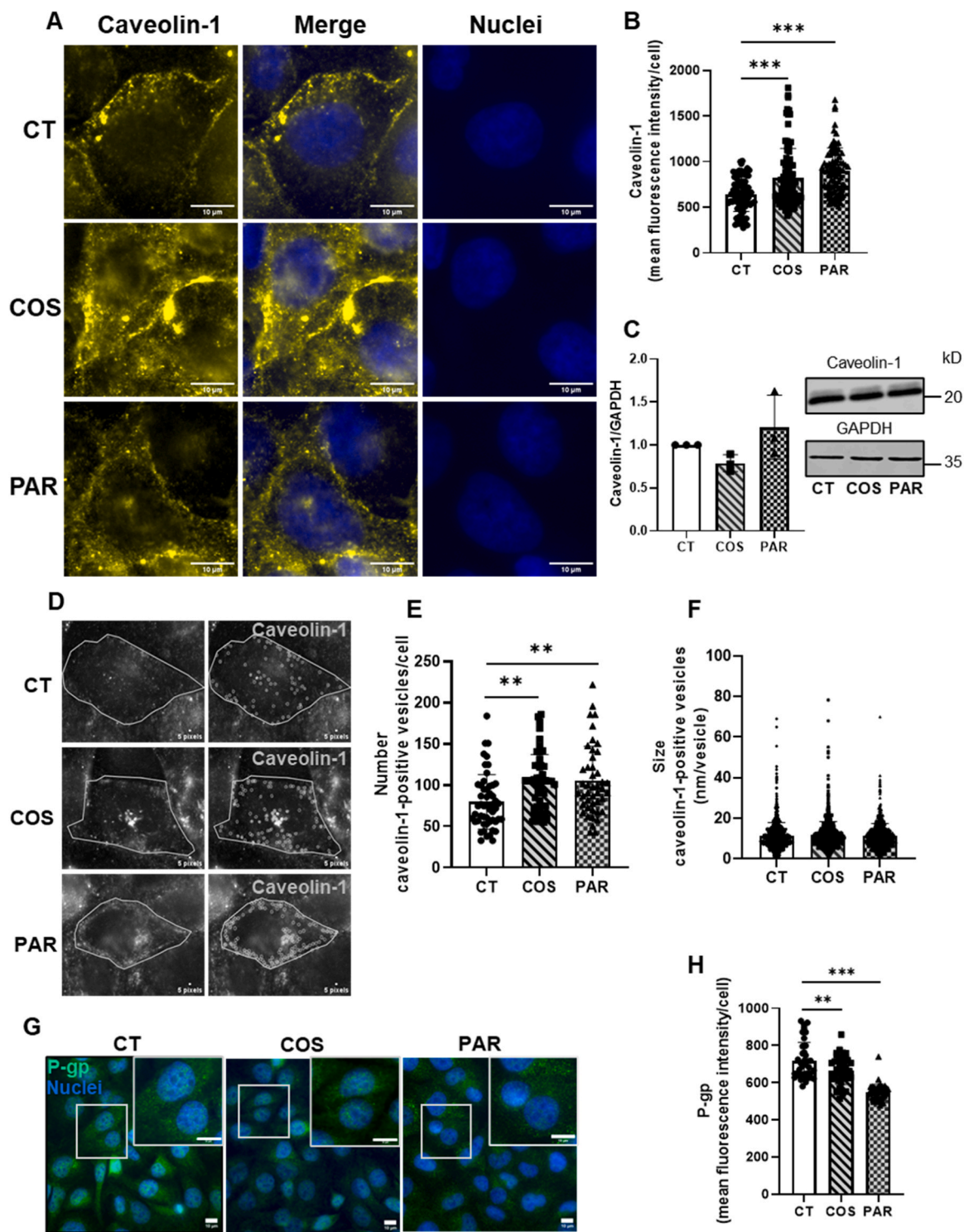


**Fig. 3.** Effect of costunolide (COS) and parthenolide (PAR) on caveolin-1 and P-gp expression in HBMECs. (A) Immunofluorescence detection of caveolin-1 (yellow) at 2 h of incubation. DAPI was used as counterstaining for nuclei. (B) Semi-quantitative analysis revealed an increase of caveolin-1 intensity at 2 h with the COS and PAR incubation. (C) Western blot analysis to detect the protein level of caveolin-1. GAPDH was used as a loading control. (D) Representative images after analysis using the spot detector tool of caveolin-1 immunofluorescence microscopy. The original and algorithm-based detected spots (grey) are shown (left and right side, respectively) and (E) semi-quantitative analysis revealed an increase in the number of vesicles with COS and PAR incubation for 2 h. Scale: 5 pixels (1 pixel=72.1 nm). (F) Size (nm) of caveolin-1-positive vesicles corresponding to detected spots in each analysed cell. Graph bars represent the mean  $\pm$  SD and the individual values for each cell (90 cells were evaluated from each condition, n = 3). (G) Immunofluorescence detection of P-gp (green). Nuclei stained with DAPI (blue). (H) Semi-quantitative analysis using the algorithm-based detected spots in the image analysis software. Graph bars represent the mean  $\pm$  SD and the individual fluorescence values for each cell (120 cells were evaluated from each condition, n = 3). One-way ANOVA with Dunnett *post hoc* was used to evaluate the significant differences between COS and PAR treatments vs control (CT). \*\*\* $p < 0.001$  or \*\* $p < 0.01$ .

### 3.4. COS and PAR promote the expression of adherens and tight junction proteins

Since the observed effects of COS and PAR in reducing Na-F permeability and increasing TEER values could be associated with effects at the levels of AJs and/or TJs proteins, we decided to explore the putative effects of both COS and PAR in paracellular hallmarks of BBB integrity, which could be related with an improvement in the barrier tightness.

For this, we opted for the evaluation of  $\beta$ -catenin, and ZO-1 as the two most representative AJs and TJs proteins, respectively, in this particular cell line [19].

Firstly, we analysed the expression of the AJ protein  $\beta$ -catenin, that is a fundamental protein to intercellular adhesion involved in supporting cadherin association and regulating out-in signalling processes [9]. No significant changes were detected in  $\beta$ -catenin expression with the treatment of COS and PAR for 2 h (Fig. 4A, C). By contrast, after 6 h of incubation, an increased  $\beta$ -catenin expression, mainly in the cell membrane, was observed for treatment with COS, which was corroborated by the corresponding semi-quantitative analysis ( $p < 0.05$  compared with the CT cells, Fig. 4B). However, the expression protein levels of  $\beta$ -catenin by both COS and PAR at 6 h, were significantly higher ( $p < 0.001$ ) than CT cells (Fig. 4D).

On the other hand, TJs serve as a boundary between the compositionally distinct apical and basolateral plasma membrane domains of HBMECs. Since ZO-1 is a TJs protein with a key role in BBB properties [9], we explored how COS and PAR could affect to the expression of this protein.

Concerning ZO-1, it can be appreciated the existence of more membrane gaps (yellow arrows) in the CT cells comparatively to the ones treated with COS or PAR after 2 and 6 h of incubation (Fig. 4E, F), supporting the observations that the fluorescent intensity of membrane ZO-1 in the cells treated with PAR or COS remained more stable and with fewer gaps. The semi-quantitative analysis of the number of gaps per cell confirmed that both COS and PAR reduced the membrane ZO-1-related gaps at 6 h (Fig. 4F). Nonetheless, already at 2 h, COS showed a trend to decrease the number of gaps-related ZO-1, whilst PAR showed a significant reduction ( $p < 0.05$ ). Regarding the ZO-1 protein expression, both COS and PAR showed a significant increase at 2 and 6 h compared with CT cells (Fig. 4G, H).

Important to notice, the effects were different in terms of timing with the incubation of the compounds. We observed that these STLs produced a reduction in ZO-1-related gaps at 2 and 6 h with a consequent higher expression of ZO-1, explaining the observed reduction of Na-F permeability at the 2 and 6 h (Fig. 1D, E). Moreover,  $\beta$ -catenin expression was only significantly increased by COS and PAR for prolonged time of exposure tested (6 h), which is in agreement with the higher TEER values observed at 6 h (Fig. 1F).

Collectively, our data supports the role that COS and PAR have in boosting barrier properties *via* modulation of TJs and AJs proteins.

## 4. Discussion

In recent decades, there has been an increasing demand for developing effective novel drugs from natural products with less side effects and more potency than conventional synthetic molecules. The first step towards achieving this goal would be to identify molecules from a structural diversity and bioactivities found in nature that could be used as starting points for optimization. Targeting brain cells through crossing the BBB and, mechanistic insight into how transport is governed could lead to improved therapies. In the present work, we showed for the first time that different STLs are brain permeable compounds using an *in vitro* validated BBB system [20]. These results are in agreement with the predicted parameters BBB scores of these compounds using an *in silico* tool [8]. One of the most useful parameters to predict the BBB permeability of a small compound is its brain/blood partition

coefficient (QPlogBB) value, which must be in the range of  $-3$  to  $1.2$ . Matos et al. reported the QPlogBB sequence obtained was as follows COS and PAR, as the more permeable compounds, whereas DHLC, LC, DHLCP, LCP were similar among them [8]. These results are consistent with our *in vitro* results, showing higher BBB transport for COS and PAR. However, the QlogBB only reflects the passive diffusion of the compounds, and the potential active transport of these compounds is not accounted, raising the interest to better understand if other mechanisms of transport, as caveolae-mediated transcytosis could take part. Importantly, COS and PAR have already been described as neuroprotective compounds against neurological damages [7]. To the best of our knowledge, this is the first study which indicates the significant ability of COS and PAR to cross the BBB.

In our study, we showed that out of the six evaluated STLs, only COS and PAR decreased the Na-F permeability and increased the TEER values in HBMECs at  $5 \mu\text{M}$  after short incubation periods (2 and 6 h). We postulate that these observed differences may be related, at least partially, with the dissimilar structures of these molecules. In this sense, COS and PAR are germacranolide-type precursors molecules, which have a different structure than the guaianolide-type STLs, namely LC, LCP, DHLC and DHLCP. The chemical structure of COS and PAR, which contain two rings, are less oxygenated and with a lower molecular weight compared with the other studied STLs, potentially explaining the differences in the BBB permeability and in the ability of decreasing the Na-F permeability observed with both compounds. Despite the effects of these STLs on BBB integrity have not been explored so far, many natural compounds from the terpene class displayed therapeutic benefits through the protective effects in BBB models. For instance, salvinorin A, a terpenoid, has been shown to prevent BBB leakage in a rat model of middle cerebral artery occlusion and in HBMECs with oxygen-glucose deprivation [21]. Another example is dihydroartemisinin, a derivative of artemisinin, which is also a STL compound, described to be involved in the pathogenesis of sepsis-associated encephalopathy either in a mouse sepsis model and in a tumour necrosis factor  $\alpha$  (TNF- $\alpha$ )-stimulated human cerebral microvessel endothelial cells (hCMEC)/D3 cell line. The described decrease of BBB permeability by dihydroartemisinin was concomitant with an increase of the expression on the TJs protein occludin, both in animals and in cells [22]. In a recent study using a BBB model from rat primary cells the drug fasudil, a vasodilator for the treatment of cerebral vasospasm, has shown its ability to decrease the Na-F permeability at 1 and  $10 \mu\text{M}$  after 24 h of treatment, with a consequent increase in TEER values, and an increase of the expression levels of TJs and AJs proteins. These effects in the BBB cells appear to be directly related with the reducing endothelial injury elicited in acute ischemic stroke [23]. Our results support all these observations and reinforce the role that STLs, as BBB permeant compounds, may have not only as neuroprotective but also by promoting BBB tightness.

In this study we also have described for the first time the formation of GSH conjugates from STLs in human endothelial cells from brain capillaries. The conjugation to glutathione was previously shown to affect STLs bioactivity. In particular, the presence of the exomethylene moiety would be behind the ability to deplete cellular thiols [24]. Importantly to mention, no conjugation was observed for DHLC and DHLCP, which is in line with the fact that the exomethylene moiety in these compounds is reduced, meaning that it is not available for this conjugation [24]. The role of GSH in the formation of glutathione S-conjugates is a well-known pathway for the membrane transport of the multidrug resistance-associated proteins' (MRP) substrates and a critical step in the elimination of many endogenous and exogenous molecules [15]. In a previous study, GSH metabolites were not detected in Caco-2 cells using the same 6 STLs investigated in this study [8]. However, these authors and previous reports suggest that the detected cysteine conjugates may result from GSH conjugates formed in the cells and then hydrolysed by the brush border membrane enzymes [8,25]. Once GSH conjugates are formed by the cells, the exportation from the cell is carried out mainly by MRPs, in order to control the cellular redox status, delivery of cysteine,

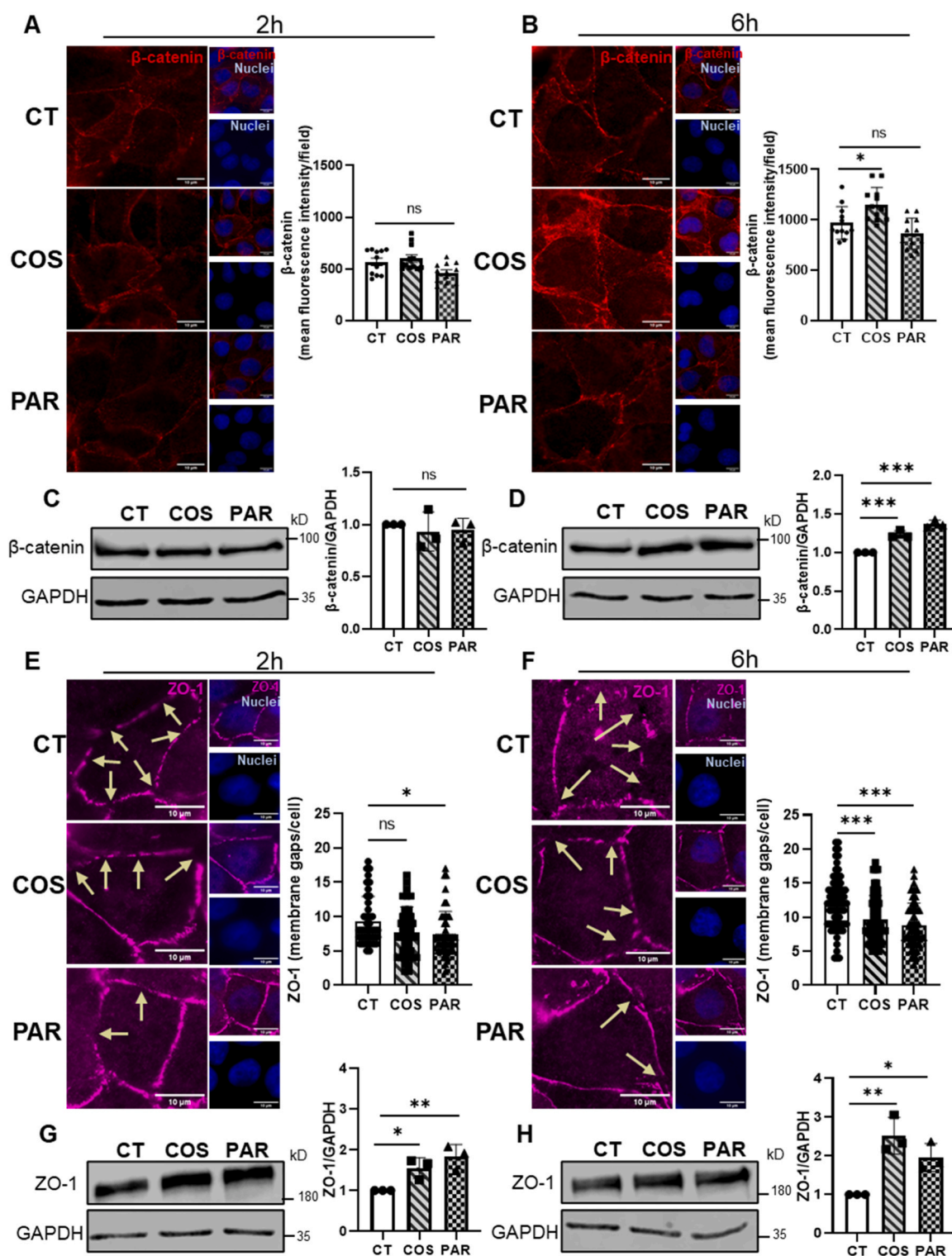


**Fig. 4.** Effect of costunolide (COS) and parthenolide (PAR) on  $\beta$ -catenin and ZO-1 in HBMECs. Immunofluorescence detection and semi-quantitative analysis of  $\beta$ -catenin expression (red) at 2 (A) and 6 h (B) of incubation, respectively. Graph bars represent the mean  $\pm$  SD and the individual fluorescence values for each field (4 fields for each condition, 10 cells/field,  $n = 3$ ). Western blot analysis to detect the protein level of  $\beta$ -catenin at 2 (C) and 6 h (D) of incubation, respectively. Immunofluorescence detection of the gaps-related (yellow arrows) ZO-1 (magenta) and semi-quantitative analysis at 2 (E) and 6 h (F) of incubation, respectively. Graph bars represents the mean  $\pm$  SD and the individual fluorescence values for each cell (120 cells were evaluated from each condition,  $n = 3$ ). Western blot analysis to detect the protein level of ZO-1 at 2 (G) and 6 h (H) of incubation, respectively. DAPI was used as counterstaining for nuclei in all fluorescence microscopy imaging. Scale bar: 10  $\mu$ m. One-way ANOVA Dunnett *post hoc* was used to evaluate the significant differences between COS or PAR vs control (CT). \* $p < 0.05$ , \*\* $p < 0.01$  and \*\*\* $p < 0.001$ . GAPDH was used as a loading control in the Western blots.

export of signalling molecules, elimination of xenobiotics and reactive metabolic intermediates, as well as to control cell differentiation, proliferation, and apoptosis [15,25].

One important mechanism of transport towards the brain is transcytosis in which caveolin-1 is a fundamental protein as the main protein constituent of caveolae [26]. Some molecules such as albumin, insulin, and lipidic molecules are known to undergo endothelial transcytosis enhancing caveolae vesicles formation [27]. Moreover, previous studies have described a physical interaction between P-gp with caveolin-1, and that the interaction leads to a down-regulation of P-gp function [17]. Although the precise mechanism of this interaction remains controversial, the role of caveolin-1 as scaffolding protein with a consequent down-regulation in the sequestered proteins, is well-described [26]. Thus, we may speculate that the increase of caveolin-1-positive vesicles observed in the presence of COS and PAR could not only support brain uptake of STLs but also be somehow related with the reduction of P-gp observed in our study. It should be pointed out that direct interaction has been reported to occur between caveolin-1 and P-gp, forming a detergent-insoluble complex that localizes within the caveolar membrane and will remain in membrane fraction of the protein extract [17, 28]. In this regard, under our assay conditions we would lose caveolin-1 and P-gp complex signal in the western blot, since we just used a general lysis buffer with a mild detergent (e.g., 1 % Triton-X). In fact, according to previous works [17] a specific fractionation process is required to evaluate the real protein levels corresponding to P-gp and caveolin-1 complex, that remains in the insoluble membrane fractions. Indeed, we detected an increase of caveolin-1-positive vesicles by immunofluorescence and a steady level of soluble caveolin-1 after COS and PAR treatments by WB, suggesting that both compounds may be affecting caveolin-1 vesicles formation, possibly *via* an increase in its synthesis or by the inhibition of its degradation. Nevertheless, additional information about the direct interaction between the P-gp and caveolin-1 in the presence of COS and PAR will require further studies.

Importantly to mention, caveolae vesicle formation in the BBB cells reflects an enhancement of the transport of a wide range of molecules [27], raising the possibility that even transport to the brain of nucleic acids, nanoparticles, and other molecules, could be enhanced by COS and PAR treatments. Transcytosis is normally actively suppressed in brain endothelial cells to ensure barrier integrity; therefore this process is dynamically regulated during development and disease [12]. Having small molecules like STLs that have the capacity to modulate this mechanism could constitute a promising strategy to facilitate brain therapeutics.

Finally, the increase observed with COS and PAR in the expression of the AJs and TJs proteins could mitigate the BBB damage associated with numerous harmful processes that occur in brain diseases since these proteins are key players in BBB homeostasis and valuable indicators of barrier integrity. Once there are no reports about the activity of STLs in those proteins, we can only compare our results with previous studies where other natural small molecules or terpene-like structures were evaluated. In this regard, an *in vivo* study reported that the intraperitoneally administration of the pentacyclic triterpenoid, oleanolic acid, reduced the permeability of BBB and relieved brain edema by increasing protein expression of TJs and AJs in rats [29]. On the other hand, Guo et al. reported bilobalide (terpene trilactone compound) changed the ultrastructure of TJs with no changes in the protein expression levels [30]. For other small molecules (e.g., polyphenols), studies both in *in vitro* and *in vivo* models have reported their beneficial effects in the BBB integrity by increasing these proteins. For instance, quercetin-3-O-galactoside was shown to protect against BBB injuries induced by either oxidative stress or angiotensin II-induced apoptosis, by increasing the expression of ZO-1 in the BBB [31]. Moreover, the administration of vanillin exerted an increment of ZO-1 levels with consequent neuroprotection on neonatal rats by alleviating oxidative stress damage and preserving BBB integrity [32]. Therefore, our results open the door to explore whether COS and PAR could boost BBB properties and mitigate

brain damage from traumatic and nontraumatic injuries in the brain. Finally, it should be pointed out the differences observed between COS and PAR increased ZO-1 expression at only 2 h while an increase in  $\beta$ -catenin expression was observed only after 6 h of incubation. Interestingly, evidences support COS and PAR potential to interact with opioid receptors and modulate their activity [33,34]. Although it is just a matter of speculation, previous studies have shown that activation of opioid receptors can upregulate expression of ZO-1 in BBB endothelial cells leading to increased barrier function [35], which may help to explain (at least partially) a faster action of these compounds in ZO-1 than on  $\beta$ -catenin expression. Overall, this study provides a step forward for future studies to unravel the role of these STLs against systemic and brain inflammation.

## 5. Conclusions

The present data show that the natural small molecules STLs have the capacity to cross the BBB endothelium. Further molecular analysis revealed that both COS and PAR increased the protein levels of AJs and TJs proteins, namely  $\beta$ -catenin and ZO-1, respectively. COS and PAR decreased the paracellular permeability in the BBB, increasing ZO-1 at short and longer time of incubation and reducing the number of ZO-1 membrane gaps, whereas the effects in  $\beta$ -catenin were seen at longer time of exposition. Another important finding is that COS and PAR lead to an increment in caveolin-1 vesicles formation with a concomitant decrease of P-gp transporter.

Overall, COS and PAR can be considered novel compounds for future *in vivo* studies that can reinforce their use as co-adjuvants and/or nutraceuticals for brain disorders. The structural diversity of STLs found in the plant kingdom is immense and with increasing knowledge on their biosynthesis, these can be produced *via* recombinant techniques using microbes or in planta. In the near future, more advances in its pharmacokinetics and in the nanotechnology of STLs formulations should be pursued.

## CRedit authorship contribution statement

**María Ángeles Ávila-Gálvez:** Conceptualization, Methodology and Investigation, formal analysis, Writing – original draft, Writing – review & editing. **Daniela Marques:** Methodology and Investigation, Writing – review & editing. **Inês Figueira:** Methodology and Investigation, Writing – review & editing. **Katarina Cankar:** Methodology and Investigation, formal analysis, Writing – original draft, Writing – review & editing. **Dirk Bosch:** Writing – review & editing. **Maria Alexandra Brito:** Writing – review & editing. **Cláudia Nunes dos Santos:** Conceptualization, Project administration, Funding acquisition, Writing – review & editing.

## Declaration of Competing Interest

The authors declare that they have no known competing financial interests or personal relationships that could have appeared to influence the work reported in this paper.

## Data availability

Data will be made available on request.

## Acknowledgements

This work was supported by the EU Horizon 2020 research & innovation programme (H2020-NMBP-BIO-2017) (grant number 760891). iNOVA4Health Research Unit (LISBOA-01-0145-FEDER-007344), which is co funded by Fundação para a Ciência e Tecnologia (FCT) / Ministério da Ciência e do Ensino Superior, through national funds, and by FEDER under the PT2020 Partnership Agreement, is acknowledged.

CNS acknowledges European Research Council (ERC) under the European Union's Horizon 2020 research and innovation program under grant agreement No 804229. Authors would like to acknowledge FCT for financial institutional support (UIDB/04138/2020 and UIDP/04138/2020) and support of DM (2021.05505. BD) and IF (2022.00151. CEECIND).

## Appendix A. Supporting information

Supplementary data associated with this article can be found in the online version at [doi:10.1016/j.biopha.2023.115413](https://doi.org/10.1016/j.biopha.2023.115413).

## References

- [1] K. Cankar, J.C. Hakkert, R. Sevenier, E. Campo, B. Schipper, C. Papastolopoulou, K. Vahabi, A. Tissier, P. Bundock, D. Bosch, CRISPR/Cas9 targeted inactivation of the kaunilolide synthase in chicory results in accumulation of costunolide and its conjugates in taproots, *Front. Plant Sci.* 13 (2022), <https://doi.org/10.3389/fpls.2022.940003>.
- [2] M.S. Matos, J.D. Anastácio, C.N. dos Santos, Sesquiterpene lactones: promising natural compounds to fight inflammation, *Pharmaceutics* 13 (2021), <https://doi.org/10.3390/pharmaceutics13070991>.
- [3] W. Ding, C. Cai, X. Zhu, J. Wang, Q. Jiang, Parthenolide ameliorates neurological deficits and neuroinflammation in mice with traumatic brain injury by suppressing STAT3/NF- $\kappa$ B and inflammasome activation, *Int. Immunopharmacol.* 108 (2022), 108913, <https://doi.org/10.1016/j.intimp.2022.108913>.
- [4] H. Weng, L. He, J. Zheng, Q. Li, X. Liu, D. Wang, Low oral bioavailability and partial gut microbiotic and phase II metabolism of brussels/witloof chicory sesquiterpene lactones in healthy humans, *Nutrients* 12 (2020) 1–12, <https://doi.org/10.3390/nu12123675>.
- [5] C.J. García, D. Beltrán, F.A. Tomás-Barberán, Human gut microbiota metabolism of dietary sesquiterpene lactones: untargeted metabolomics study of lactucopicrin and lactucin conversion in vitro and in vivo, *Mol. Nutr. Food Res.* 64 (2020), <https://doi.org/10.1002/mnfr.202000619>.
- [6] T. An, H. Yin, Y. Lu, F. Liu, The emerging potential of parthenolide nanoformulations in tumor therapy, *Drug Des. Dev. Ther.* 16 (2022) 1255–1272, <https://doi.org/10.2147/DDDT.S355059>.
- [7] S. Peng, Y. Hou, J. Yao, J. Fang, Activation of Nrf2 by costunolide provides neuroprotective effect in PC12 cells, *Food Funct.* 10 (2019) 4143–4152, <https://doi.org/10.1039/C8FO02249F>.
- [8] M.S. Matos, J.D. Anastácio, J.W. Allwood, D. Carregosa, D. Marques, J. Sungurtas, G.J. McDougall, R. Menezes, A.A. Matias, D. Stewart, C.N. dos Santos, Assessing the intestinal permeability and anti-inflammatory potential of sesquiterpene lactones from chicory, *Nutrients* 12 (2020) 1–20, <https://doi.org/10.3390/nu12113547>.
- [9] F.L. Cardoso, D. Brites, M.A. Brito, Looking at the blood–brain barrier: molecular anatomy and possible investigation approaches, *Brain Res Rev.* 64 (2010) 328–363, <https://doi.org/10.1016/j.brainresrev.2010.05.003>.
- [10] E.A. Chowdhury, B. Noorani, F. Alqahtani, A. Bhalerao, S. Raut, F. Sivandzade, L. Cucullo, Understanding the brain uptake and permeability of small molecules through the BBB: a technical overview, *J. Cereb. Blood Flow. Metab.* 41 (2021) 1797–1820, <https://doi.org/10.1177/0271678x20985946>.
- [11] M.E. Morris, V. Rodriguez-Cruz, M.A. Felmler, SLC and ABC transporters: expression, localization, and species differences at the blood–brain and the blood–cerebrospinal fluid barriers, *AAPS J.* 19 (2017) 1317–1331, <https://doi.org/10.1208/s12248-017-0110-8>.
- [12] R. Daneman, A. Prat, The blood–brain barrier, *Cold Spring Harb. Perspect. Biol.* 7 (2015), <https://doi.org/10.1101/cshperspect.a020412>.
- [13] J. Chen, X. Wang, J. Hu, J. Du, C. Dordoe, Q. Zhou, W. Huang, R. Guo, F. Han, K. Guo, S. Ye, L. Lin, X. Li, FGF20 Protected against BBB disruption after traumatic brain injury by upregulating junction protein expression and inhibiting the inflammatory response, *Front. Pharm.* 11 (2021), <https://doi.org/10.3389/fphar.2020.590669>.
- [14] I. Figueira, G. Garcia, R.C. Pimpão, A.P. Terrasso, I. Costa, A.F. Almeida, L. Tavares, T.F. Pais, P. Pinto, M.R. Ventura, A. Filipe, G.J. McDougall, D. Stewart, K.S. Kim, I. Palmela, D. Brites, M.A. Brito, C. Brito, C.N. Santos, Polyphenols journey through blood–brain barrier towards neuronal protection, *Sci. Rep.* 7 (2017), <https://doi.org/10.1038/s41598-017-11512-6>.
- [15] N. Ballatori, S.M. Krance, R. Marchan, C.L. Hammond, Plasma membrane glutathione transporters and their roles in cell physiology and pathophysiology, *Mol. Asp. Med.* 30 (2009) 13–28, <https://doi.org/10.1016/j.mam.2008.08.004>.
- [16] D. Carlisi, A. de Blasio, R. Drago-Ferrante, R. di Fiore, G. Buttitta, M. Morreale, C. Scerri, R. Vento, G. Tesoriere, Parthenolide prevents resistance of MDA-MB231 cells to doxorubicin and mitoxantrone: the role of Nrf2, *Cell Death Discov.* 3 (2017) 17078, <https://doi.org/10.1038/cddiscovery.2017.78>.
- [17] S. Barakat, M. Demeule, A. Pilorget, A. Régina, D. Gingras, L.G. Baggetto, R. Béliveau, Modulation of p-glycoprotein function by caveolin-1 phosphorylation, *J. Neurochem* 101 (2007) 1–8, <https://doi.org/10.1111/j.1471-4159.2006.04410.x>.
- [18] D. Fu, Where is it and how does it get there - intracellular localization and traffic of P-glycoprotein, *Front Oncol.* 3 (2013) 321, <https://doi.org/10.3389/fonc.2013.00321>.
- [19] I. Palmela, H. Sasaki, F.L. Cardoso, et al., Time-dependent dual effects of high levels of unconjugated bilirubin on the human blood–brain barrier lining, *Front Cell Neurosci.* 6 (2012) 22, <https://doi.org/10.3389/fncel.2012.00022>.
- [20] D.E. Eigenmann, G. Xue, K.S. Kim, A.V. Moses, M. Hamburger, M. Oufir, Comparative study of four immortalized human brain capillary endothelial cell lines, hCMEC/D3, hBMEC, TY10, and BB19, and optimization of culture conditions, for an in vitro blood–brain barrier model for drug permeability studies, *Fluids Barriers CNS* 10 (2013) 33, <https://doi.org/10.1186/2045-8118-10-33>.
- [21] J. Xin, X. Ma, W. Chen, W. Zhou, H. Dong, Z. Wang, F. Ji, Regulation of blood–brain barrier permeability by Salvinorin A via alleviating endoplasmic reticulum stress in brain endothelial cell after ischemia stroke, *Neurochem. Int.* 149 (2021), 105093, <https://doi.org/10.1016/j.neuint.2021.105093>.
- [22] F. Liu, J. Liu, H. Xiang, Z. Sun, Y. Li, X. Li, Y. Liu, J. Liu, Dihydroartemisinin protects blood–brain barrier permeability during sepsis by inhibiting the transcription factor SNAI1, *Clin. Exp. Pharmacol. Physiol.* 49 (2022) 979–987, <https://doi.org/10.1111/1440-1681.13683>.
- [23] K. Sato, S. Nakagawa, Y. Morofuji, Y. Matsunaga, T. Fujimoto, D. Watanabe, T. Izumo, M. Niwa, F.R. Walter, J.P. Vigh, A.R. Santa-Maria, M.A. Deli, T. Matsuo, Effects of fasudil on blood–brain barrier integrity, *Fluids Barriers CNS* 19 (2022) 43, <https://doi.org/10.1186/s12987-022-00336-w>.
- [24] Q. Liu, M. Majidi, K. Cankar, M. Goedbloed, T. Charnikhova, F.W.A. Verstappen, R. C.H. de Vos, J. Beekwilder, S. van der Krol, H.J. Bouwmeester, Reconstitution of the costunolide biosynthetic pathway in yeast and *Nicotiana benthamiana*, *PLoS One* 6 (2011), e23255, <https://doi.org/10.1371/journal.pone.0023255>.
- [25] U. Thormann, R. Hänggi, M. Kreuter, G. Imanidis, Membrane transport of nobililn conjugation products and use of the extract of *Chamomilla romanae* flos influence absorption of nobililn in the Caco-2 model, *Eur. J. Pharm. Sci.* 70 (2015) 92–106, <https://doi.org/10.1016/j.ejps.2014.11.011>.
- [26] J.P.X. Cheng, B.J. Nichols, Caveolae: one function or many? *Trends Cell Biol.* 26 (2016) 177–189, <https://doi.org/10.1016/j.tcb.2015.10.010>.
- [27] B.J. Andreone, B.W. Chow, A. Tata, B. Lacoste, A. Ben-Zvi, K. Bullock, A.A. Deik, D. D. Ginty, C.B. Clish, C. Gu, Blood–brain barrier permeability is regulated by lipid transport-dependent suppression of caveolae-mediated transcytosis, *581-594.e5*, *Neuron* 94 (2017), <https://doi.org/10.1016/j.neuron.2017.03.043>.
- [28] C. Cai, J. Chen, Overexpression of caveolin-1 induces alteration of multidrug resistance in Hs578T breast adenocarcinoma cells, *Int J. Cancer* 111 (2004) 522–529, <https://doi.org/10.1002/ijc.20300>.
- [29] Y.-W. Han, X.-J. Liu, Y. Zhao, X.-M. Li, Role of Oleanolic acid in maintaining BBB integrity by targeting p38MAPK/VEGF/Src signaling pathway in rat model of subarachnoid hemorrhage, *Eur. J. Pharm.* 839 (2018) 12–20, <https://doi.org/10.1016/j.ejphar.2018.09.018>.
- [30] C. Guo, H. Wang, W. Liang, W. Xu, Y. Li, L. Song, D. Zhang, Y. Hu, B. Han, W. Wang, Y. Yang, W. Bei, J. Guo, Bilobalide reversibly modulates blood–brain barrier permeability through promoting adenosine A1 receptor-mediated phosphorylation of actin-binding proteins, *Biochem. Biophys. Res. Commun.* 526 (2020) 1077–1084, <https://doi.org/10.1016/j.bbrc.2020.03.186>.
- [31] Y.Y. Xie, Y.W. Lu, G.R. Yu, The protective effects of hyperoside on Ang II-mediated apoptosis of bEnd.3 cells and injury of blood–brain barrier model in vitro, *BMC Complement Med. Ther.* 22 (2022), <https://doi.org/10.1186/s12906-022-03635-9>.
- [32] X.B. Lan, Q. Wang, J.M. Yang, L. Ma, W.J. Zhang, P. Zheng, T. Sun, J.G. Niu, N. Liu, J.Q. Yu, Neuroprotective effect of Vanillin on hypoxic-ischemic brain damage in neonatal rats, *Biomed. Pharmacother.* 118 (2019), <https://doi.org/10.1016/j.biopha.2019.109196>.
- [33] H. Okugawa, R. Ueda, K. Matsumoto, K. Kawanishi, K. Kato, Effects of sesquiterpenoids from "Oriental incenses" on acetic acid-induced writhing and D2 and 5-HT<sub>2A</sub> receptors in rat brain, *Phytomedicine: Int. J. Phytother. Phytother.* 7 (2000) 417–422, [https://doi.org/10.1016/S0944-7113\(00\)80063-X](https://doi.org/10.1016/S0944-7113(00)80063-X).
- [34] K. Popiolek-Barczyk, W. Makuch, E. Rojewska, D. Pilat, J. Mika, Inhibition of intracellular signaling pathways NF- $\kappa$ B and MEK1/2 attenuates neuropathic pain development and enhances morphine analgesia, *Pharmacol. Rep.* 66 (2014) 845–851, <https://doi.org/10.1016/j.pharep.2014.05.001>.
- [35] M. Ji, J. Cheng, D. Zhang, Oxycodone protects cardiac microvascular endothelial cells against ischemia/reperfusion injury by binding to Sigma-1 receptor, *Bioengineered* 13 (2022) 9628–9644, <https://doi.org/10.1080/21655979.2022.2057632>.